LETTERS

High-resolution subsurface water-ice distributions on Mars

Joshua L. Bandfield[1]

Theoretical models indicate that water ice is stable in the shallow subsurface (depths of <1–2 m) of Mars at high latitudes[1–7]. These models have been mainly supported by the observed presence of large concentrations of hydrogen detected by the Gamma Ray Spectrometer suite of instruments on the Mars Odyssey spacecraft[8–10]. The models and measurements are consistent with a water-ice table that steadily increases in depth with decreasing latitude. More detailed modelling has predicted that the depth at which water ice is stable can be highly variable, owing to local surface heterogeneities such as rocks and slopes, and the thermal inertia of the ground cover[11–13]. Measurements have, however, been limited to the footprint (several hundred kilometres) of the Gamma Ray Spectrometer suite, preventing the observations from documenting more detailed water-ice distributions. Here I show that by observing the seasonal temperature response of the martian surface with the Thermal Emission Imaging System on the Mars Odyssey spacecraft[14], it is possible to observe such heterogeneities at subkilometre scale. These observations show significant regional and local water-ice depth variability, and, in some cases, support distributions in the subsurface predicted by atmospheric exchange and vapour diffusion models. The presence of water ice where it follows the depth of stability under current climatic conditions implies an active martian water cycle that responds to orbit-driven climate cycles[15–17]. Several regions also have apparent deviations from the theoretical stability level, indicating that additional factors influence the ice-table depth. The high-resolution measurements show that the depth to the water-ice table is highly variable within the potential Phoenix spacecraft landing ellipses, and is likely to be variable at scales that may be sampled by the spacecraft.

The high concentrations of water ice inferred from Gamma Ray Spectrometer (GRS) measurements[10,11] require that the water ice in the shallow subsurface on Mars be a mixture of water ice and regolith/rocky material. As a result, this subsurface water-ice/regolith mixture will have a thermal inertia similar to solid bedrock, that is, much higher than the more porous, dry, particulate regolith cover[4,7,11]. Martian high latitudes have thermal properties consistent with an extensive high-thermal-inertia layer within a few centimetres of the surface, though extremely high thermal inertia values of $>1{,}000\ \mathrm{J\,m^{-2}\,K^{-1}\,s^{-1/2}}$, which are consistent with bedrock exposed at the surface, are rare[18]. The presence of this near-surface high-inertia layer with few surface exposures is consistent with the presence of a significant ice component that is insulated by several centimetres of ground cover. Although surfaces of increased thermal inertia are present at high latitudes, these surfaces commonly have thermal inertia values of only $400–500\ \mathrm{J\,m^{-2}\,K^{-1}\,s^{-1/2}}$.

The temperature response of a material is dependent on the intensity and period of the input energy cycle in addition to the thermophysical properties of the material itself. The thickness of the surface layer that is influenced by the energy cycle (referred to as the skin depth) is proportional to the square root of the period of the cycle. Thus properties at a variety of depths can be determined from Phobos eclipse (roughly millimetre scales)[19], diurnal (centimetre scales)[20,21] and seasonal (decimetre to metre scales)[22–25] surface temperature measurements. At high latitudes, the magnitude of the seasonal energy cycle is prominent, enhancing the surface temperature effect of a buried high-inertia water-ice-rich layer. At low latitudes, the lower seasonal variation in the energy cycle results in greatly diminished sensitivities to layers beyond diurnal skin depths.

Seasonal temperature measurements from the Thermal Emission Spectrometer (TES) on the Mars Global Surveyor spacecraft clearly indicate the presence of subsurface ice at high latitudes[23–25]; however, the determination of the depth of this high-inertia ice layer is not precise. This is largely because variable surface properties (for example, surface frosts) within the 3 km resolution of TES and uncertain atmospheric properties can have significant effects on the modelled surface temperatures.

A more precise assessment of subsurface water-ice distributions can be obtained by measuring the seasonal change in relative temperatures between surfaces (Fig. 1). The high precision (in-flight measurements indicate a noise equivalent delta temperature of 1 K at 165 K) and high spatial resolution (100 m sampling) of night-time (local time of 03:30–05:30) Thermal Emission Imaging System (THEMIS) data are well suited for this application. By observing the change in relative temperatures between mid- to late-summer

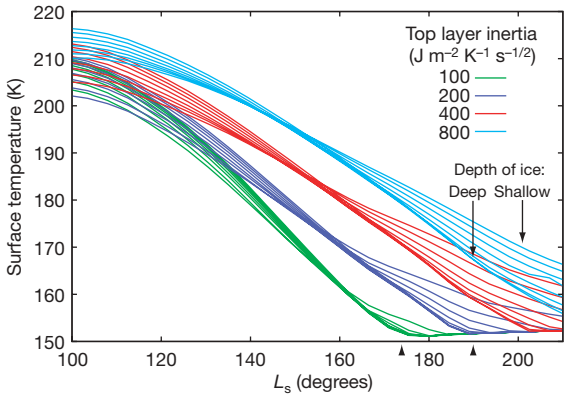

Figure 1 | Modelled temperatures for a variety of surface cover thermal inertias (top layer inertia) and ice-table depths, at 67.5°N. At this latitude, the high-inertia ice layer has little influence on surface temperatures near L_s (solar longitude) 160°, and primarily affects the rate of cooling throughout the late summer/early autumn season. Arrow points on the seasonal scale show the time of collection for the data used to generate Fig. 2. Temperatures are for a local time of 05:00, a surface albedo of 0.20 and a visible dust opacity of 0.30.

[1]School of Earth and Space Exploration, Arizona State University, Tempe, Arizona 85287-6305, USA.

and early autumn, it is possible to gain insight into the relative inertias of the surface layers and the relative depth to the high-inertia subsurface layer. The thermal inertia of the surface layer dominates the surface temperatures during the mid- to late-summer, and the change in relative temperatures between summer and early autumn is dominated by the depth of the ice layer (Fig. 1). Many uncertainties in modelling surface temperatures (for example, surface CO_2 frost, aerosol opacities, slope and albedo effects owing to low solar incidence) are avoided or largely cancel out using this method. Thus, surfaces that cool more quickly between summer and autumn have a deeper ice layer, and the slower cooling surfaces have a shallow ice layer.

The THEMIS data can be quantitatively supported by comparing the measured temperatures to those predicted by thermal models[20,21] (the model used here was developed by H. H. Kieffer). Surface and subsurface temperatures are predicted, given proper environmental input parameters as well as a one-dimensional model of surface and subsurface properties containing layers of variable-inertia regolith cover and a high-inertia ice-bedrock layer. Although real world material distributions may be more complex, this model is useful for gaining initial insight into subsurface properties. In addition, the relatively simple nature of the temperature data used here prevents the recovery of additional information from a more complex surface model. The model also predicts the maximum annual temperature of the water-ice layer. The temperature of water-ice stability is highly dependent on the role of atmospheric water vapour, and has been predicted to be 198 K with a mean annual water vapour column abundance of 10 precipitable micrometres (refs 7, 11).

Figure 2 displays seasonal temperature difference data from the Phoenix B region proposed landing site[26]. Many of the slightly lower-albedo surfaces in the region display a higher night-time (and lower daytime) temperature throughout the summer season, indicative of a higher-inertia ground cover. These observations are supported by initial Mars Reconnaissance Orbiter High Resolution Imaging Science Experiment (HiRISE) images that indicate that these regions commonly have higher rock abundances[27] that would increase the average thermal inertia of the ground cover. The rocky surfaces change temperature more slowly on diurnal timescales and more quickly on seasonal timescales than the surrounding terrain through the early autumn season (Fig. 3). This temperature response is consistent with a deeper ice table in the low-albedo regions. The measured temperatures can be matched well in the low-albedo surfaces by a ground cover with a thermal inertia of 400 J m^{-2} K^{-1} $s^{-1/2}$ with an ice-bedrock layer at >18 cm (sensitivities are low at depths of greater than ~20 cm). The seasonal temperatures of the higher-albedo surfaces can be well modelled by a ground cover thermal inertia of 200 J m^{-2} K^{-1} $s^{-1/2}$ and an ice-bedrock layer at 5 cm depth, consistent with lower-resolution measurements[25].

Similar data were processed for the Phoenix A region proposed landing site (shown in Supplementary Figs S1 and S2). In this case, regional differences in ice-table depth are clearly apparent (consistent with ice-table depths > 9 cm), but the high degree of correlation with surface morphology at the subkilometre scale is not present.

In both examples, the modelled temperatures of the bedrock-ice layers never exceed 198 K, though the two regions apparently have a different character of subsurface ice distributions at this scale. A likely cause for this difference is the relatively variable surface-cover thermal inertia present at subkilometre scales in the Phoenix region B versus region A. The modelled surfaces are consistent with current orbital, atmospheric and thermophysical equilibrium conditions and free exchange with the martian atmosphere[1–7,11–13]. This implies that ice deposition can occur in these regions by way of atmospheric vapour exchange.

Whereas near-surface ice stability generally decreases with increasing distance from the pole, local heterogeneities (such as slopes and variations in regolith cover) have a dominant effect on the local subsurface water-ice distributions[11–13]. Far more variation in the ice-table depth can appear within a small section of the proposed

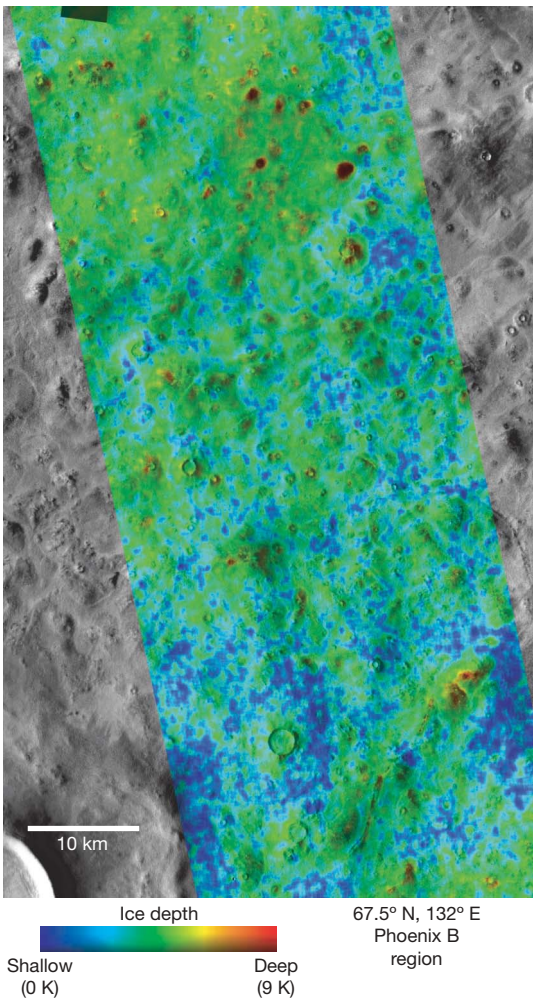

Figure 2 | Ice depth map centred near 67.5° N, 132° E (Phoenix B region proposed landing site). This map was produced by differencing the relative surface temperatures present in THEMIS night-time images I14393035 and I14705021, acquired at L_s 174° and 189°, respectively. Data are overlaid on a THEMIS visible image mosaic for morphological context. Modelled temperatures (Fig. 3) indicate that blue colours are consistent with water ice at 5 cm depth and red colours are consistent with water ice at >18 cm.

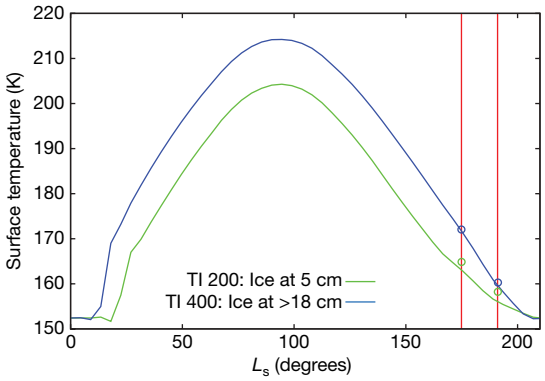

Figure 3 | Modelled temperatures at 05:00 for the surfaces shown in Fig. 2. Red vertical lines indicate the times of data acquisition, and circles are surface temperatures derived from THEMIS data. Both absolute temperatures and temperature differences between the shallow (green curve; top layer thermal inertia (TI) of 200 J m^{-2} K^{-1} $s^{-1/2}$) and deep (blue curve; top layer thermal inertia of 400 J m^{-2} K^{-1} $s^{-1/2}$) ice surfaces shown in Fig. 2 are matched well (within 5 K absolute and 2 K relative) by the model.

Phoenix landing site regions than predicted by the theoretical stabilities throughout the region based on low-resolution data sets. In addition, high-resolution images show clear indications of surface heterogeneity, implying that a highly variable ice table can be present at even smaller spatial scales than presented here.

Figure 4 displays seasonal temperature difference data in the southern hemisphere near Melea Planum. This region is marked by a smooth (at 100 m scales) layer that appears to be a remnant of a more extensive unit, rough hummocky terrain, and sand deposits that collect in local depressions. The surface thermophysical properties display little correlation with surface morphology, except where sand dune forms are present. The sand deposits have the largest amount of seasonal cooling, consistent with a relatively deep ice table compared with the surrounding terrain. Surface temperatures can be fitted with a modelled ground cover thermal inertia of 220 J m^{-2} K^{-1} s$^{-1/2}$ with ice present at >19 cm for the sand deposits (shown in Supplementary Fig. S3). The surrounding terrain surface temperatures are consistent with a ground cover inertia of 150 J m^{-2} K^{-1} s$^{-1/2}$ with ice present at 1 cm depth. Several areas displayed in Fig. 4 have an even lower degree of seasonal cooling, indicating an even shallower ice table.

The sand deposits are consistent with either an ice table limited by the 198 K temperature constraint or no ice table at all. A well-sorted sand would be highly permeable and permit free exchange of the subsurface with the atmosphere, limiting the depth of water-ice stability to where this temperature is not exceeded. In addition, if the sand is mobile, any shallow ice table would be eventually exposed to non-equilibrium temperature conditions close to the surface. Outside the sand deposits, the ice table is apparently significantly shallower than predicted by the 198 K temperature of ice stability. This could be due to either an effective seal of the ground cover that would prevent effective atmospheric exchange and/or higher local annual-mean water vapour abundances that would raise the temperature of water-ice stability. The surface temperature data could not be reasonably fitted by a model where the 198 K subsurface ice temperature constraint is preserved.

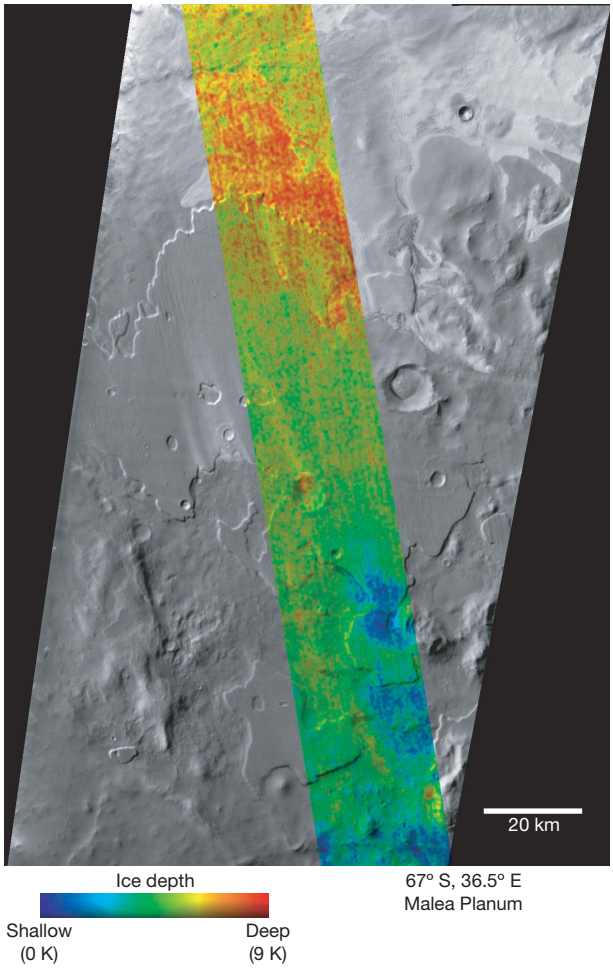

Figure 4 | Ice depth map centred near 67° S, 36.5° E. This map was produced by differencing the relative surface temperatures present in THEMIS night-time images I17904012 and I18216009, acquired at L_s 347° and 0°, respectively. Data are overlaid on a THEMIS daytime infrared image mosaic for morphological context. Low-albedo duneforms appear bright because of their warmer daytime temperatures. Modelled temperatures (Supplementary Fig. S3) indicate that blue colours are consistent with water ice at <1 cm depth, and red colours are consistent with water ice at >19 cm.

The seasonal temperature data indicate clear subsurface water-ice heterogeneity, as well as regional differences in the pattern of ice distributions. As has been noted[11–13], the nature of the ground cover has a dominant effect on the depth of stability of the water-ice table. Higher-inertia materials will have greater temperatures at depth because of their higher thermal conductivity and because their cooler daytime temperatures do not radiate the heat away as effectively as low-inertia materials. The THEMIS seasonal temperature data in the examples shown here largely support the depths of water ice predicted by theoretical models[1–7,11–13]. As also shown by the GRS measurements, the presence of ice at its current stability limits may indicate that large changes in stability predicted to accompany orbital variations drive an active water cycle between the poles, regolith and atmosphere[5,15,16].

There appear to be instances where the presence of ice does not, however, follow its limit of stability. Because the sensitivity of the temperature data to the presence of a high-inertia layer is limited to a couple of decimetres, regions where ice is predicted to be greater than ~20 cm may indeed have no subsurface ice at all. In addition, the presence of the shallow ice in the southern hemisphere example (Fig. 4) appears to clearly violate the assumed ice stability conditions. The detailed distribution of water ice in martian high latitudes appears to be complex, with controlling factors beyond those predicted by vapour diffusion models. As noted in ref. 28, there are reasonable geologic situations that would prevent or considerably slow the exchange of water between atmosphere and regolith. This supports the notion that shallow water ice may be present on Mars at lower latitudes than predicted by vapour diffusion models.

The regions presented here were limited by the fortuitous acquisition of at least two images of the same surface during specific seasons and local times. More directed targeting would allow a number of regions to be studied, so as to assemble a more complete picture of the martian subsurface water-ice distributions.

METHODS SUMMARY

THEMIS data were calibrated using methods described elsewhere[14,29]. An additional correction was made for potential focal plane temperature drift between acquisition of the image and calibration data. Because of the temperature stability of the martian atmosphere during these seasons (<1–2 K inter-annual variation[30]), the resulting calibrated THEMIS data are accurate to within 5 K at 160 K.

Data were converted to brightness temperature from the 12.6 μm THEMIS band 9. Because of the relatively low atmospheric opacity, low surface–atmosphere temperature contrast, and high surface emissivity for the observations used in this study, brightness temperatures are within 1–2 K of surface kinetic temperature. Temperature images taken over a single surface at two seasons were subtracted from each other in order to isolate the relative temperature changes between surfaces. This subtraction also cancels the absolute temperature uncertainties discussed above.

Modelled temperatures were fitted to the measured data by manually adjusting regolith cover thermal inertia and depth to ice-bedrock layer until the predicted surface temperatures fall within the uncertainties of the measured THEMIS surface temperatures. Although it is possible to automate a fitting routine[24,25], it is difficult to adjust the weighting of the factors to produce an intelligent convergence. In addition, uncertainties in the model, and in surface and atmospheric properties fed into the model, preclude a more accurate

determination than what can be produced manually. As a result, the model fits are used as an example of consistency with surface temperature measurements, but uncertainties in ice-table depth and regolith cover inertia are poorly understood. Sensitivity to the depth of the ice-bedrock layer is greatest where the layer is shallow, the surface cover thermal inertia is low, and the latitude is 40–90°.

Full Methods and any associated references are available in the online version of the paper at www.nature.com/nature.

Received 2 December 2006; accepted 26 March 2007.

1. Leighton, R. R. & Murray, B. C. Behavior of carbon dioxide and other volatiles on Mars. *Science* **153,** 136–144 (1966).
2. Fanale, F. P., Salvail, J. R., Zent, A. P. & Postawko, S. E. Global distribution and migration of subsurface ice on Mars. *Icarus* **67,** 1–18 (1986).
3. Zent, A. P., Fanale, F. P., Salvail, J. R. & Postawko, S. E. Distribution and state of H_2O in the high-latitude shallow subsurface of Mars. *Icarus* **67,** 19–36 (1986).
4. Paige, D. A. The thermal stability of near-surface ground ice on Mars. *Nature* **356,** 43–45 (1992).
5. Mellon, M. T. & Jakosky, B. M. The distribution and behavior of Martian ground ice during past and present epochs. *J. Geophys. Res.* **100,** 11781–11799 (1995).
6. Jakosky, B. M., Zent, A. P. & Zurek, R. W. The Mars water cycle: Determining the role of exchange with the regolith. *Icarus* **130,** 87–95 (1997).
7. Boynton, W. V. *et al.* Distribution of hydrogen in the near surface of Mars: Evidence for subsurface ice deposits. *Science* **297,** 81–85 (2002).
8. Schorghofer, N. & Aharonson, O. Stability and exchange of subsurface ice on Mars. *J. Geophys. Res.* **110,** E5003, doi:10.1029/2004JE002350 (2005).
9. Feldman, W. C. *et al.* Global distribution of near-surface hydrogen on Mars. *J. Geophys. Res.* **109,** E9006, doi:10.1029/2003JE002160 (2004).
10. Mitrofanov, I. G. *et al.* Soil water content on Mars as estimated from neutron measurements by the HEND instrument onboard the 2001 Mars Odyssey Spacecraft. *Solar Syst. Res.* **38,** 253–257 (2004).
11. Mellon, M. T., Feldman, W. C. & Prettyman, T. H. The presence and stability of ground ice in the southern hemisphere of Mars. *Icarus* **169,** 324–340 (2004).
12. Sizemore, H. G. & Mellon, M. T. Effects of soil heterogeneity on martian ground-ice stability and orbital estimates of ice table depth. *Icarus* **185,** 358–369 (2006).
13. Aharonson, O. & Schorghofer, N. Subsurface ice on Mars with rough topography. *J. Geophys. Res.* **111,** E11007, doi:10.1029/2005JE002636 (2006).
14. Christensen, P. R. *et al.* The Thermal Emission Imaging System (THEMIS) for the Mars 2001 Odyssey Mission. *Space Sci. Rev.* **110,** 85–130 (2004).
15. Haberle, R. M. & Jakosky, B. M. Sublimation and transport of water from the north residual polar cap on Mars. *J. Geophys. Res.* **95,** 1423–1437 (1990).
16. Jakosky, B. M., Henderson, B. G. & Mellon, M. T. Chaotic obliquity and the nature of the Martian climate. *J. Geophys. Res.* **100,** 1579–1584 (1995).
17. Head, J., Mustard, J., Kreslavsky, M., Milliken, R. & Marchant, D. Recent ice ages on Mars. *Nature* **426,** 797–802 (2003).
18. Edwards, C. S., Bandfield, J. L., Christensen, P. R. & Fergason, R. L. Global distribution of bedrock on Mars using THEMIS high resolution thermal inertia. *Eos* 158 (Fall Mtg), abstr. P21C–0158 (2005).
19. Betts, B. H., Murray, B. C. & Svitek, T. Thermal inertias in the upper millimeters of the Martian surface derived using Phobos' shadow. *J. Geophys. Res.* **100,** 5285–5296 (1995).
20. Kieffer, H. H. *et al.* Thermal and albedo mapping of Mars during the Viking primary mission. *J. Geophys. Res.* **82,** 4249–4291 (1977).
21. Mellon, M. T., Jakosky, B. M., Kieffer, H. H. & Christensen, P. R. High-resolution thermal inertia mapping from the Mars Global Surveyor Thermal Emission Spectrometer. *Icarus* **148,** 437–455 (2000).
22. Paige, D. A., Bachman, J. E. & Keegan, K. D. Thermal and albedo mapping of the polar regions of Mars using Viking thermal mapper observations: 1. North polar region. *J. Geophys. Res.* **99,** 25959–25991 (1994).
23. Titus, T. N., Kieffer, H. H. & Christensen, P. R. Exposed water ice discovered near the south pole of Mars. *Science* **299,** 1048–1051 (2003).
24. Armstrong, J. C., Titus, T. N. & Kieffer, H. H. Evidence for subsurface water ice in Korolev crater, Mars. *Icarus* **174,** 360–372 (2005).
25. Titus, T. N., Prettyman, T. P. & Colaprete, A. Thermal characterization of the three proposed Phoenix landing sites. *Lunar. Planet. Sci. Conf.* 37, abstr. 2161 (2006).
26. Arvidson, R. E. *et al.* Overview of Mars exploration program 2007 Phoenix mission landing site selection. *Lunar. Planet. Sci. Conf.* 37, abstr. 1328 (2006).
27. Polygonal terrain in the northern plains. ⟨http://marsoweb.nas.nasa.gov/HiRISE/hirise_images/TRA/TRA_000828_2495/⟩ (2006).
28. Jakosky, B. M. *et al.* Mars low-latitude neutron distribution: Possible remnant near-surface water ice and a mechanism for its recent emplacement. *Icarus* **175,** 58–67 (2005).
29. Bandfield, J. L., Rogers, D., Smith, M. D. & Christensen, P. R. Atmospheric correction and surface spectral unit mapping using Thermal Emission Imaging System data. *J. Geophys. Res.* **109,** E10008, doi:10.1029/2004JE002289 (2004).
30. Smith, M. D. Interannual variability in TES atmospheric observations of Mars during 1999–2003. *Icarus* **167,** 148–165 (2004).

Supplementary Information is linked to the online version of the paper at www.nature.com/nature.

Acknowledgements Thanks to P. Christensen, R. Fergason, H. Kieffer, C. Edwards, R. Luk, K. Bender, and J. Hill for data processing and targeting help and discussions.

Author Information Reprints and permissions information is available at www.nature.com/reprints. The author declares no competing financial interests. Correspondence and requests for materials should be addressed to the author (joshband@asu.edu).

METHODS

THEMIS data were calibrated using methods described elsewhere[14,29]. An additional correction was performed by adjusting the data number of all bands until the measured radiance in THEMIS band 10 matched that predicted by TES data within the 15 μm CO_2 fundamental. This corrects for potential focal plane temperature drift between acquisition of the image and calibration data. Because of the temperature stability of the martian atmosphere during these seasons (<1–2 K inter-annual variation[30]), the resulting calibrated THEMIS data are accurate to within 5 K at 160 K.

Data were converted to brightness temperature from the 12.6 μm THEMIS band 9 using a look-up table of Planck radiances convolved with the THEMIS band 9 filter response. Because of the relatively low atmospheric opacity ($\tau < 0.05$), low surface–atmosphere temperature contrast (<20 K), and high surface emissivity ($\varepsilon > 0.98$) at 12.6 μm for the observations used in this study, brightness temperatures are within 1–2 K of surface kinetic temperature.

THEMIS images were selected by the following criteria: (1) all image incidence angles are >90°. This ensures that albedo and surface slopes have little effect on the surface temperatures in the pre-dawn images; (2) all images have average band 9 brightness temperatures >155 K and no regions contain significant areas at CO_2 condensation temperatures (~148 K); (3) all images were acquired in the late summer or early autumn season, and each image pair was acquired in the same year at a similar local time with a separation of at least 10° L_s. The image pairs used for this work were I14393035−I14705021 (Fig. 2), I17904012−I18216009 (Fig. 4), and I14401005−I14713023 (Supplementary Fig. S1).

To produce the depth maps, the two temperature images were subtracted from each other and the level was adjusted to make the surface with the least amount of cooling equal zero. This isolates the relative temperature changes between surfaces and cancels the absolute temperature uncertainties discussed above. On the basis of the model results displayed in Fig. 1, this subtraction also provides the relative rate of seasonal cooling, which is largely independent of surface cover thermal inertia and highly dependent on the burial depth of the subsurface water ice.

Modelled temperatures were fitted to the measured data by manually adjusting regolith cover thermal inertia and depth to ice-bedrock layer until the predicted surface temperatures fall within the uncertainties of the measured THEMIS surface temperatures. The ice-bedrock layer used the properties for density, thermal conductivity, and heat capacity listed in ref. 11. Although it is possible to automate a fitting routine[23,24], it is difficult to adjust the weighting of the factors to produce an intelligent convergence. In addition, uncertainties in the model and surface and atmospheric properties fed into the model preclude a more accurate determination than what can be produced manually. As a result, the model fits are used as an example of consistency with surface temperature measurements, but uncertainties in ice-table depth and regolith cover inertia are poorly understood. However, dependence on several factors such as heterogeneous surfaces (lateral mixtures of rocks and fine particulates), surface albedo, and atmospheric dust properties were tested and found to have little effect on the predicted temperatures at the local time and season of image acquisition for the data used in this study. For example, a surface composed of rocks and soil will simply raise the thermal inertia of the surface cover relative to a homogeneous soil and have little effect on the modelled rate of seasonal cooling.

The sensitivity of the measurements to the presence and depth of water ice is dependent on three main factors; the ground cover thermal inertia, the depth of the ice, and latitude. The thermal model used in this work divides layers on the basis of units of skin depth rather than absolute depth in order to achieve similar levels of temperature precision for a variety of thermal inertia values. Because the skin depth is proportional to the thermal inertia, the model will have twice the vertical resolution for a surface cover thermal inertia of 200 versus 400 $J\,m^{-2}\,K^{-1}\,s^{-1/2}$, for example. The surface temperature influence of a high-inertia ice-rich layer is reduced by a factor of ~2–3 with each doubling of its depth. For example, at 65° N with a surface cover thermal inertia of 220 $J\,m^{-2}\,K^{-1}\,s^{-1/2}$, an ice layer at 5 cm will have up to a 7.5 K effect during the autumn season versus 4 K at 10 cm and 1.3 K at 20 cm. Lastly, the latitude influences the magnitude of seasonal variation in energy input to the surface. A surface cover thermal inertia of 220 $J\,m^{-2}\,K^{-1}\,s^{-1/2}$ and an ice layer at 5 cm will have up to an 8–10 K effect during the autumn season at latitudes of 40–90° versus <3 K at latitudes of <30°.

The combination of these effects greatly reduces the uncertainty in water-ice depths where the depths are shallow, the surface cover thermal inertia is low, and the latitude is >40°. For example, with a surface cover thermal inertia of 150 $J\,m^{-2}\,K^{-1}\,s^{-1/2}$ and a water-ice depth of 1 cm (similar to surfaces shown in Fig. 4), a change to 0.5 cm in depth will cause up to a 3 K difference in surface temperature during the autumn season. With a surface cover thermal inertia of 300 $J\,m^{-2}\,K^{-1}\,s^{-1/2}$ and a water-ice depth of 14 cm, a change to 20 cm in depth is required to cause the same 3 K difference in surface temperature.

SUPPLEMENTARY INFORMATION

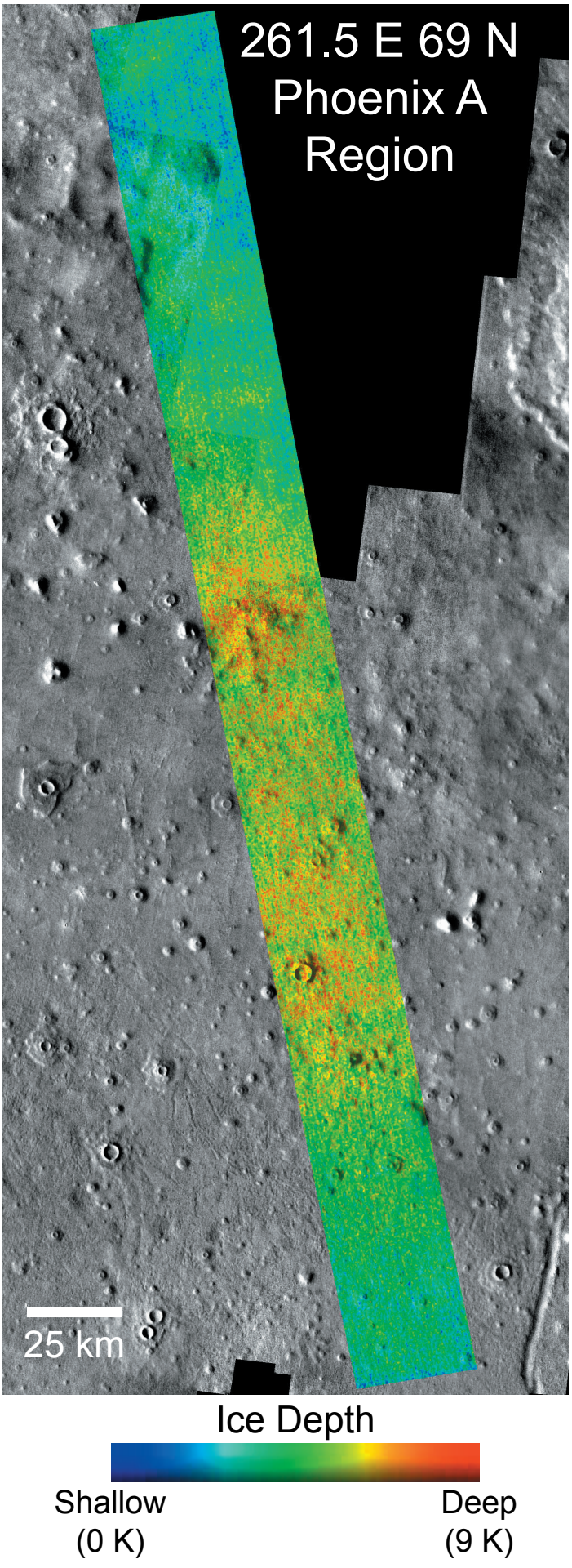

Figure S1. Ice depth map centred near 67.5 N 132 E. This map was produced by differencing the relative surface temperatures present in THEMIS night time images I14401005 and I14713023, acquired at Ls 175 and 190 respectively. Data is overlaid on a THEMIS daytime infrared image mosaic for morphological context. Modelled temperatures (Figure S2) indicate that blue colours are consistent with water-ice at 9 cm and red colours are consistent with water-ice at >20 cm.

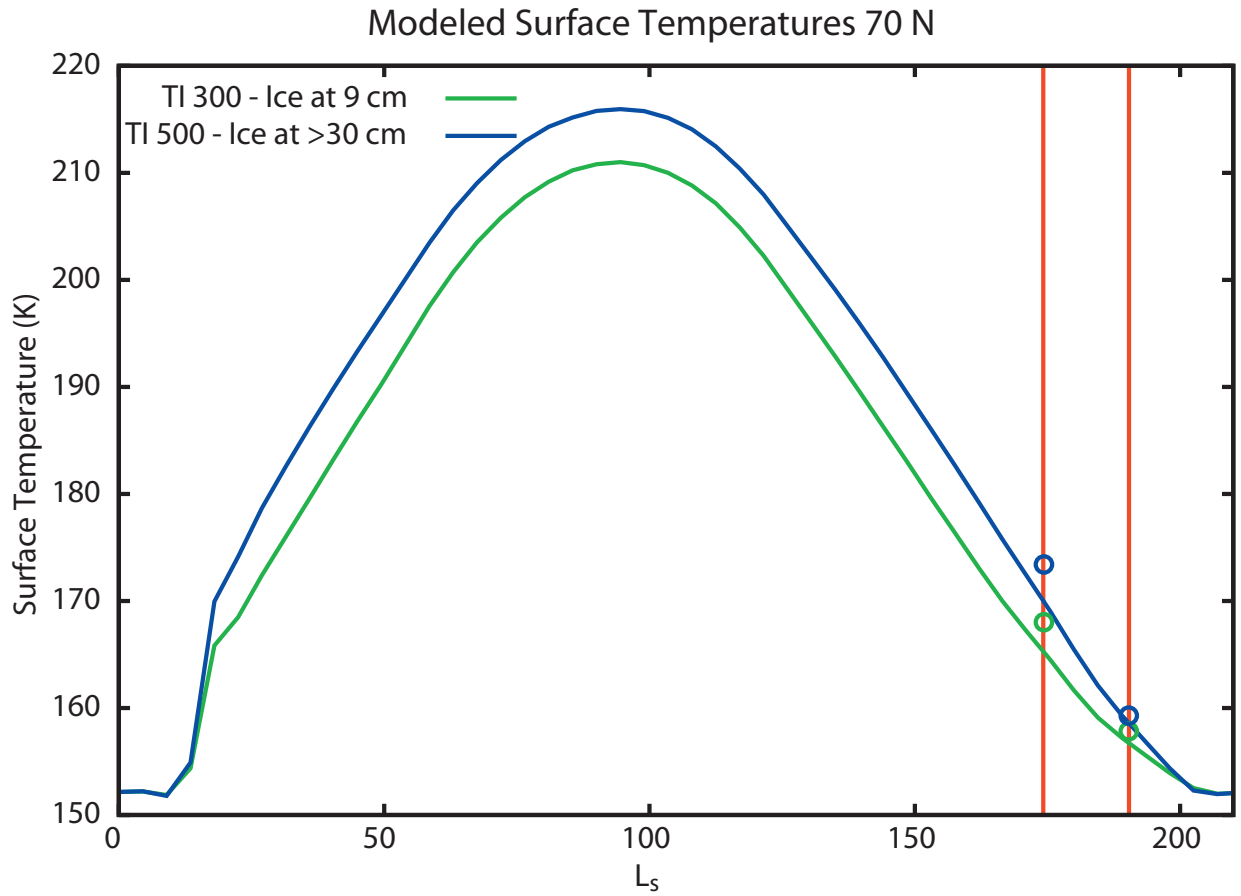

Figure S2. Modelled 5AM temperatures for the surfaces shown in Figure S1. Red vertical lines indicate the times of data acquisition and circles are surface temperatures derived from THEMIS data. Both absolute temperatures and temperature differences between the shallow and deep ice surfaces shown in Figure S1 are matched well (within 5 K absolute and 2 K relative) by the model.

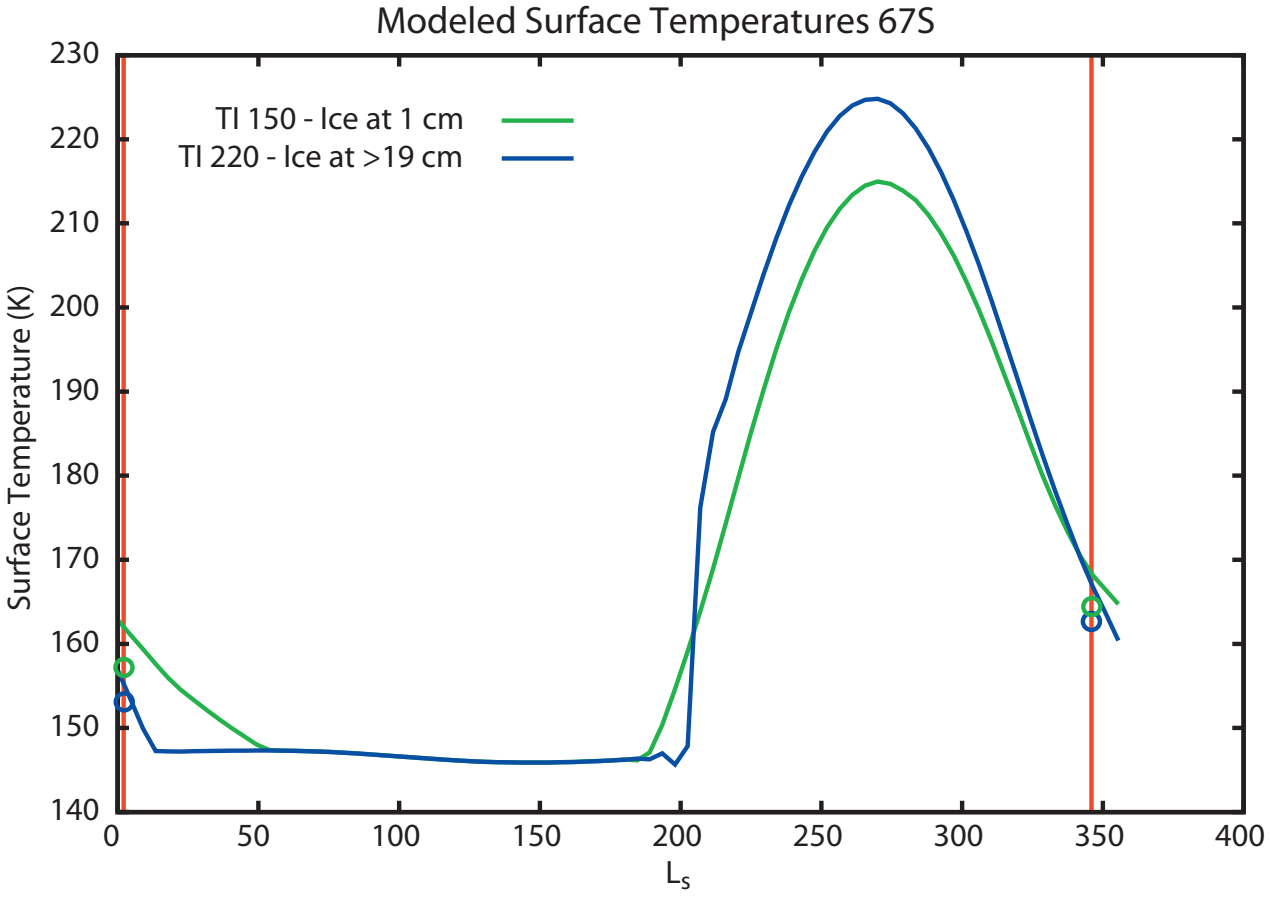

Figure S3. Modelled 5AM temperatures for the surfaces shown in Figure 4. Red vertical lines indicate the times of data acquisition and circles are surface temperatures derived from THEMIS data, similar to Figure S2.